JACS
JOURNAL OF THE AMERICAN CHEMICAL SOCIETY

Article

pubs.acs.org/JACS

Near-Infrared Lasing from Small-Molecule Organic Hemispheres

Xuedong Wang,[†,‡] Qing Liao,[§] Hui Li,[†,‡] Shuming Bai,[†,‡] Yishi Wu,[†] Xiaomei Lu,[§] Huaiyuan Hu,[∥] Qiang Shi,[†] and Hongbing Fu*[,†,§,⊥]

[†]Beijing National Laboratory for Molecular Sciences (BNLMS), Institute of Chemistry, Chinese Academy of Sciences, Beijing 100190, P. R. China

[‡]University of Chinese Academy of Sciences, Beijing 100049, P. R. China

[§]Beijing Key Laboratory for Optical Materials and Photonic Devices, Department of Chemistry, Capital Normal University, Beijing 100048, P. R. China

[∥]Department of Chemistry, The University of Alabama, Tuscaloosa, Alabama 35487, United States

[⊥]Collaborative Innovation Center of Chemical Science and Engineering, Tianjin 300072, P. R. China

Supporting Information

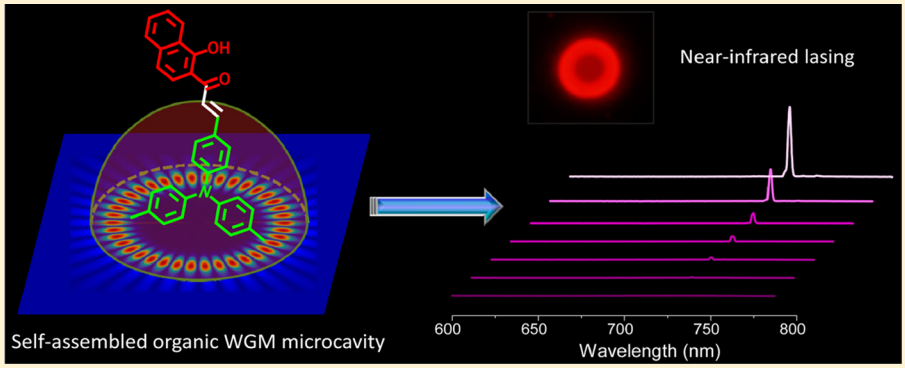

ABSTRACT: Near-infrared (NIR) lasers are key components for applications, such as telecommunication, spectroscopy, display, and biomedical tissue imaging. Inorganic III−V semiconductor (GaAs) NIR lasers have achieved great successes but require expensive and sophisticated device fabrication techniques. Organic semiconductors exhibit chemically tunable optoelectronic properties together with self-assembling features that are well suitable for low-temperature solution processing. Major blocks in realizing NIR organic lasing include low stimulated emission of narrow-bandgap molecules due to fast nonradiative decay and exciton−exciton annihilation, which is considered as a main loss channel of population inversion for organic lasers under high carrier densities. Here we designed and synthesized the small organic molecule (*E*)-3-(4-(di-*p*-tolylamino)phenyl)-1-(1-hydroxynaphthalen-2-yl)prop-2-en-1-one (DPHP) with amphiphilic nature, which elaborately self-assembles into micrometer-sized hemispheres that simultaneously serves as the NIR emission medium with a photoluminescence quantum efficiency of ∼15.2%, and the high-Q (∼1.4×10^3) whispering gallery mode microcavity. Moreover, the radiative rate of DPHP hemispheres is enhanced up to ∼1.98×10^9 s^{-1} on account of the exciton-vibrational coupling in the solid state with the J-type molecular-coupling component, and meanwhile the exciton−exciton annihilation process is eliminated. As a result, NIR lasing with a low threshold of ∼610 nJ/cm^2 is achieved in the single DPHP hemisphere at room temperature. Our demonstration is a major step toward incorporating the organic coherent light sources into the compact optoelectronic devices at NIR wavelengths.

INTRODUCTION

Organic solid-state lasers (OSSLs) have been a significant research subject since the first demonstration of laser oscillation in 1960s.[1−7] Among all kinds of organic laser materials, π-conjugated organic small molecules are of foremost interest due to the large binding energy (>200 meV) of Frenkel excitons,[8] the high photoluminescence (PL) quantum efficiency η,[9] the compatibility with plastic substrates,[10] and the flexibility in molecular design.[11,12] Notably, OSSLs have been demonstrated in three primary colors of blue, green, and red, which are essential for the realization of full-color laser displays.[7,13] Furthermore, there is a large demand for near-infrared (NIR) OSSLs, because of their potential applications in night vision devices, bioimaging, and optical telecommunications.[14] Nevertheless, the development of NIR OSSLs is still hampered by the low PL quantum efficiency associated with NIR gain materials, owing to (i) the intrinsic fast nonradiative decay of low band gap organic semiconductors, and (ii) the serious concentration quenching as a result of strong $\pi-\pi$ interactions in the solid-

Received: March 24, 2015
Published: July 7, 2015

DOI: 10.1021/jacs.5b03051
J. Am. Chem. Soc. 2015, 137, 9289−9295

state.[15,16] Moreover, exciton−exciton annihilation, which occurs under intensely optical or electrical excitation,[17−19] will further severely impair the optical gain and thus impede the lasing action.[20−22] Therefore, the development of efficient organic NIR gain media with optimized energy levels that help obtain high PL quantum efficiency and avoid the exciton−exciton loss channel is imperative.

For the achievement of lasers, the optical microcavity provides feedback for light amplification and defines the spatial and spectral coherence of the laser beam.[23] Therefore, various kinds of structures and fabrication techniques have been investigated to provide microcavity for lasing oscillation, including Fabry−Pérot (FP) cavity,[24] distributed brag reflector (DBR) resonator,[25] and photonic crystal[26] as well as whispering gallery mode (WGM) microcavity.[27] Among them, WGM microcavity features low cavity loss and small mode volume (V) for integration of miniaturized devices.[23,28] Over the past decades, the fabrication technology of optical microcavities has been significantly advanced but requires complicated, high-temperature, and costly production processes. As a matter of fact, small molecule organic semiconductor materials inherently offer a bottom-up optical microcavity fabrication approach through the low-temperature solution-based self-assembly method.[29,30]

Herein, we report that room-temperature NIR lasing is achieved in the microsized organic solid-state hemispheres, which are facilely self-assembled from a π-conjugated organic small molecule of (E)-3-(4-(di-p-tolylamino)phenyl)-1-(1-hydroxynaphthalen-2-yl)prop-2-en-1-one (DPHP). Several unique aspects of this work are worth highlighting up front: (i) the incorporation of intramolecular hydrogen bond (IHB) can increase the conjugation length of coplanar π-electron system, thus providing a narrow bandgap (600−850 nm) and a high PL quantum efficiency (~15.2%) for the solid-state DPHP; (ii) the propeller-shape-like molecular geometry of DPHP determines a ladder molecular arrangement with J-type coupling component, which is helpful for enhancing the radiative decay rate k_r (~1.98×10^9 s^{-1}) in the solid state; (iii) the "bottom-up" synthesized organic hemispheres provide a high-Q (~1.4×10^3) WGM microcavity for laser action due to the molecularly smooth surfaces; and (iv) the ultrafast radiative transition suppresses the exciton−exciton annihilation nonradiative process under the high carrier density, which allows our organic solid-state NIR lasing with a low threshold of ~610 nJ/cm^2.

RESULTS AND DISCUSSION

We designed and synthesized an organic π-conjugated small molecule of DPHP through the classical Claisen−Schmidt condensation reaction (Scheme 1).

Figure 1a presents the absorption (blue) and fluorescence (red) spectra of DPHP (top panel) in dichloromethane (DCM). The absorption and fluorescence maxima occur at 468 and 635 nm, respectively. For comparison, the steady-state absorption and fluorescence spectra of (E)-3-(4-(di-p-tolylamino)phenyl)-1-(1-methoxynaphthalen-2-yl)prop-2-en-1-one (DPMP) are also shown in the bottom panel of Figure 1a. As compared with DPHP, the hydrogen of hydroxyl group is replaced by a methyl group in DPMP to exclude the IHB. It can be seen from Figure 1a that both the absorption and fluorescence spectra of DPHP are red-shifted from those of DPMP. This is because the IHB in DPHP can increase the conjugation length of the coplanar π-electron system, as indicated in Figure 1b.[31] Meanwhile, the fluorescence maximum (~650 nm) of DPHP powder is also red-shifted from that (~575 nm) of DPMP powder (Figure S8, Supporting Information). Besides, the PL quantum efficiency (~14.5%) of DPHP powder is much larger than that (~1.3%) of DPMP powder. Thus, the incorporation of IHB within DPHP leads to the planarization of the molecular geometry and then gives rise to a much narrower bandgap with a high PL quantum efficiency in the solid state.

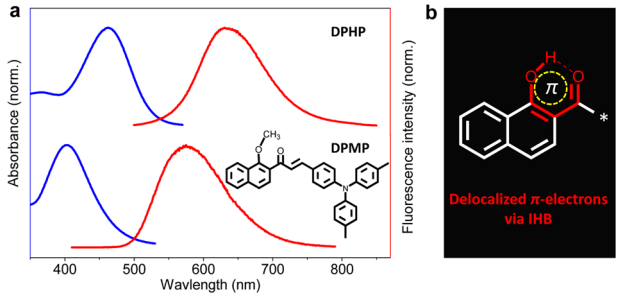

Figure 1. (a) Absorption (blue) and PL (red) spectra of DPHP (top panel) and DPMP (bottom panel) in DCM. The structure of DPMP is shown. (b) A graphical scheme of the extended π-system via the IHB within DPHP molecule.

We found that the PL spectra of DPHP solutions are red-shifted with the increasing polarity of the solvents (Figure S7 and Table S3). This solvatochromism can be ascribed to the donor−acceptor (D−A) characteristics of DPHP molecule as indicated by the obvious change of electric-cloud between the highest occupied molecular orbital (HOMO) and the lowest unoccupied molecular orbital (LUMO, Figure S9a).[16] In order to investigate the optical properties of monomeric-state DPHP without this solvatochromism, we carried out a solid-state 'dilution' experiment by doping DPHP with 2 wt % in PMMA film.[32] Figure 2a depicts the absorption (dashed line) and the PL (solid line) spectra of DPHP-doped PMMA film (top panel) and DPHP single crystal (bottom panel). The absorption maximum of the doped film is about 461 nm, which is close to that of solutions (Figure S7 and Table S3). Moreover, the PL maximum of the doped film is at ~596 nm, as there is no solvent relaxation associated with the excited state of DPHP in the doped PMMA film. Meanwhile, the doped film showed a PL quantum efficiency of ~10.3% larger than that of the solution (~0.23%, Table S3). This enhancement of PL can be attributed to the restriction of intramolecular rotations (RIR) in 'solid solution'.[32,33] As compared with the doped film, the DPHP single crystals exhibit the red-shifted absorption and PL emission. The DPHP single crystal exhibits a broad PL spectra spanning from far-red to NIR wavelength (600−850 nm) with 0−0, 0−1, and 0−2 vibronic transitions at 643, 687, and 756 nm, respectively.

Taking a closer look of DPHP molecule, the propeller-shape-like triarylamine part (top left inset of Figure 2d) can effectively prevent the face-to-face interaction between DPHP molecules

Scheme 1. Synthetic Route of DPHP Organic Molecule

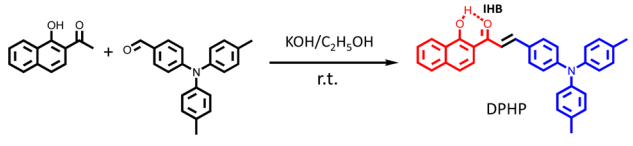

DOI: 10.1021/jacs.5b03051
J. Am. Chem. Soc. 2015, 137, 9289−9295

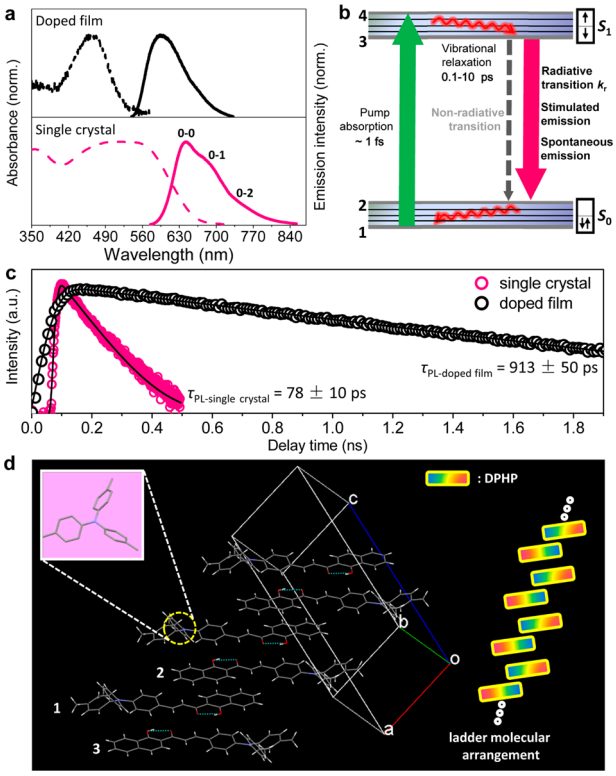

Figure 2. (a) Absorption (dashed line) and PL (solid line) spectra of the DPHP 2 wt % doped PMMA film (top panel) and the single crystal (bottom panel). (b) Schematic representation of the four-level system. (c) Time-resolved PL decay transient of the DPHP single crystal (red) and the 2 wt % doped PMMA film (black). (d) J-type ladder packing-mode of DPHP in single crystal. The left top inset presents the propeller-shape-like molecular geometry of DPHP.

(Figure 2d) in single crystal, resulting in the slippery packing mode with a relatively high solid-state quantum efficiency η of ~15.2% for the narrow-band organic single crystal solid state. Monoclinic DPHP single crystals (CCDC no. 1045866, Table S1) belong to the space group of $P2_1/c$, with cell parameters of a = 10.0 Å, b = 10.1 Å, c = 25.1 Å, $\alpha = \gamma = 90°$, and $\beta = 97.6°$. The PL lifetimes τ_{PL} of DPHP single crystal and doped PMMA film, extracted from the time-resolved PL data (Figure 2c), are ~78 and ~913 ps. The obtained quantum efficiencies and lifetimes of DPHP samples are summarized in Table 1.

Table 1. Photophysical Parameters of DPHP Samples

sample	η (%)	τ (ps)	k_r (× 10^9 s^{-1})
doped film[a]	10.3 ± 1.0	913 ± 50	0.11 ± 0.02
single crystal	15.2 ± 1.0	78 ± 10	1.98 ± 0.37

[a]2 wt % doped PMMA film.

Therefore, the radiative decay rate k_r of DPHP doped film is calculated to be $k_{\text{doped film}} = (0.11 \pm 0.02) \times 10^9$ s^{-1}, according to the equation, $k_r = \eta/\tau$.[34] Unprecedentedly, the radiative rate k_r of DPHP single-crystal reaches as high as $(1.98 \pm 0.37) \times 10^9$ s^{-1}, which is 1 order of magnitude higher than the previously reported organic laser active materials, such as ~0.28 × 10^9 s^{-1} of anthracene crystal[6] and ~0.15 × 10^9 s^{-1} of MEH-PPV.[35] Both the enhanced radiative decay rate (~1.98 × 10^9 s^{-1}) and the red-shifted absorption/PL spectra of DPHP single-crystal, as compared with those of DPHP monomeric state in the doped film, reveal the J-type coupling component in the solid-state aggregates.[36,37]

To further investigate this ultrafast radiative transition in the solid-state aggregates, the excitonic coupling of DPHP molecules in structure cell of single-crystal (such as molecules 1 and 2 in Figure 2d) is given by the dipole−dipole interaction based on the eq 1:

$$V_{d-d}^{12} = \frac{1}{4\pi\varepsilon_0}\kappa\frac{|\mu_1||\mu_2|}{R^3} \quad (1)$$

where $|\mu_1|$ and $|\mu_2|$ are the magnitudes of the transition dipoles (obtained from TD-DFT calculation at CAM-B3LYP/6-311G level) and R is the center-to-center separation.[38] And the orientation factor κ can be expressed by the equation:

$$\kappa \equiv \hat{r}_1\cdot\hat{r}_2 - 3(\hat{r}_1\cdot\hat{R})(\hat{r}_2\cdot\hat{R}) \quad (2)$$

where $\hat{R}$ is a unit vector connecting the centers of the transition moments, and the $\hat{r}_1$ and $\hat{r}_2$ are unit vectors in the directions of the transition dipoles.[38] The dipole−dipole interaction for aggregated dimer formed by molecules 1 and 2 in Figure 2d is calculated to be 1395 cm^{-1}, which is a characteristic of strong J-type coupling.[36−38] And the simulated absorption spectra of the 1,2-dimer (Figure S9) is indeed red-shifted than that of the monomer, in accordance with J-type coupling. Note that the dipole−dipole interaction for dimer formed by molecules 1 and 3 in Figure 2d is calculated to be −719 cm^{-1}, indicating a relatively weak H-type coupling effect. In overall, this slippery ladder arrangement (the right part of Figure 2d) of DPHP molecules supports more J-aggregation characteristics.[36] The numerically calculated absorption and PL spectra (Figure S11a,b) of a 4 × 2 × 2 aggregates (Figure S11c) are red-shifted from that of the DPHP monomer. This is in agreement with our experimental spectra (Figure 2a).[37] As a matter of fact, as compared with the radiative decay rate of monomer state in doped film (~0.11 × 10^9 s^{-1}, Table 1), the enhanced radiative rate of solid-state DPHP hemispheres is up to ~1.98 × 10^9 s^{-1}, on account of the strong exciton-vibrational coupling in the J-type aggregated solid state.[37] Therefore, this ultrafast radiative transition strongly promises the efficient optical gain for the population inversion, which indicates this small organic π-conjugated molecule DPHP is an excellent gain candidate for NIR lasing emission.

DPHP organic hemispheres are fabricated by using a facile solution self-assembly method at room temperature.[39] In a typical fabrication process, DPHP (16.5 mg) is dissolved in the solvent of CH_2Cl_2 (1.0 mL). To this solution (~35.2 mmol/L), 0.5 mL of H_2O was added under vigorous stirring. Then this mixture is dropped onto a clean glass substrate (Brand: Electron Microscopy Sciences), and a number of circular droplets take shape due to the oleophobic effect and the surface tension force of CH_2Cl_2 (Figure 3b).[40,41] It should be noted that CH_2Cl_2 is not miscible with water and is heavier with a greater density than that of water. Therefore, water molecules would distribute uniformly on the hydrophilic surface of glass substrate, forming a coating layer that clads separated CH_2Cl_2 droplets (Figure S12). DPHP molecules are amphiphilic in nature and are entirely dissolved in CH_2Cl_2 droplets. We speculate that the triarylamine group of DPHP molecules is dissolving in the CH_2Cl_2 phase and the 2-formyl-1-naphthol group forms a hydrogen bond with water molecules on the outer surface of CH_2Cl_2 droplets (Figure 3b). Finally, with the solvents evaporating, the hemispherical solid microstructures

DOI: 10.1021/jacs.5b03051
J. Am. Chem. Soc. 2015, 137, 9289−9295

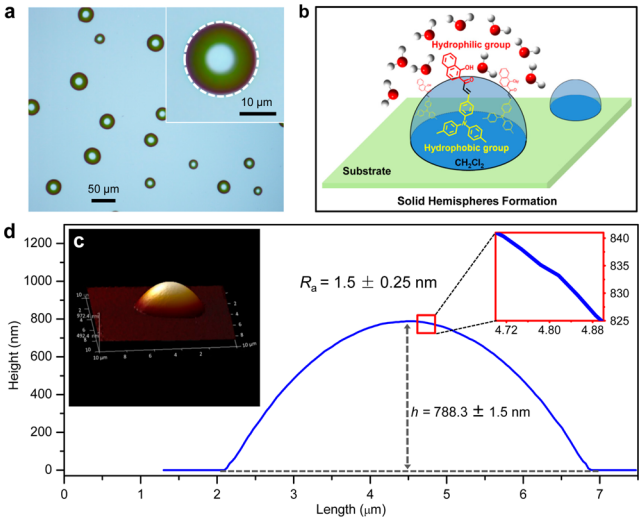

Figure 3. (a) The optical image of these self-assembled DPHP hemispheres. Scale bar is 50 μm. Inset: the magnified optical image of one hemisphere with a scale bar of 10 μm. (b) A representative picture of the hemispherical microcavity formation. (c) AFM observation of one typical hemisphere. (d) The corresponding height file of hemisphere in Figure 2c. The magnification of the height profile shows that the average surface roughness R_a of hemispheres is measured to be ~1.5 nm.

are formed. It also should be mentioned here that the water could slow down the evaporation of CH_2Cl_2 during the formation of organic hemispheres. Thus, through adjusting the volume of H_2O, organic DPHP hemispheres with different sizes can be obtained (Figure S13). Especially, when the DPHP solution (in DCM, 35.2 mmol/L) without H_2O was dropped onto the glass substrate, only the smaller hemispheres with the average diameter of ~2.5 μm were fabricated (Figure S13d).

Figure 3a presents the optical image of these as-prepared DPHP microstructures, which are presented as a hemispherical morphology, whose diameter D ranges from 2.0 to 26.5 μm (Figure S15). And the magnified optical image of an individual hemisphere is shown in the top right inset of Figure 3a. From this image, we can find that these self-assembled microstructures possess a hemispherical shape and the trace line of the structure boundary is perfectly circular. The X-ray diffraction (XRD) peaks of the DPHP hemispheres correspond with that of the DPHP single crystals (Figure S16). This suggests that these as-prepared organic DPHP hemispheres feature the same crystal phase as the single crystal.[42] Figure 3c,d demonstrates the atomic force microscope (AFM) image and the corresponding height file of one typical DPHP microstructure, which confirms the well-defined hemispherical shape. Moreover, the magnification of the height profile (blue line, in the right inset of Figure 3d) illustrates that the average surface roughness of hemispheres is as low as 1.5 ± 0.25 nm, which indicates the perfectly smooth surface at the optical level. These as-prepared hemispheres exhibit strongly far-red and NIR PL under the excitation of unfocused UV light (330–380 nm), with a bright ring at the circumference of the structure in the magnified image (Figure S17). Meanwhile, the PL quantum efficiency of these as-prepared DPHP hemispheres is as high as ~15.5%, which is close to that of the DPHP single crystals (~15.2%). Thus, these self-assembled DPHP organic hemispheres can simultaneously function as the NIR active medium and the efficient optical microcavity.[29]

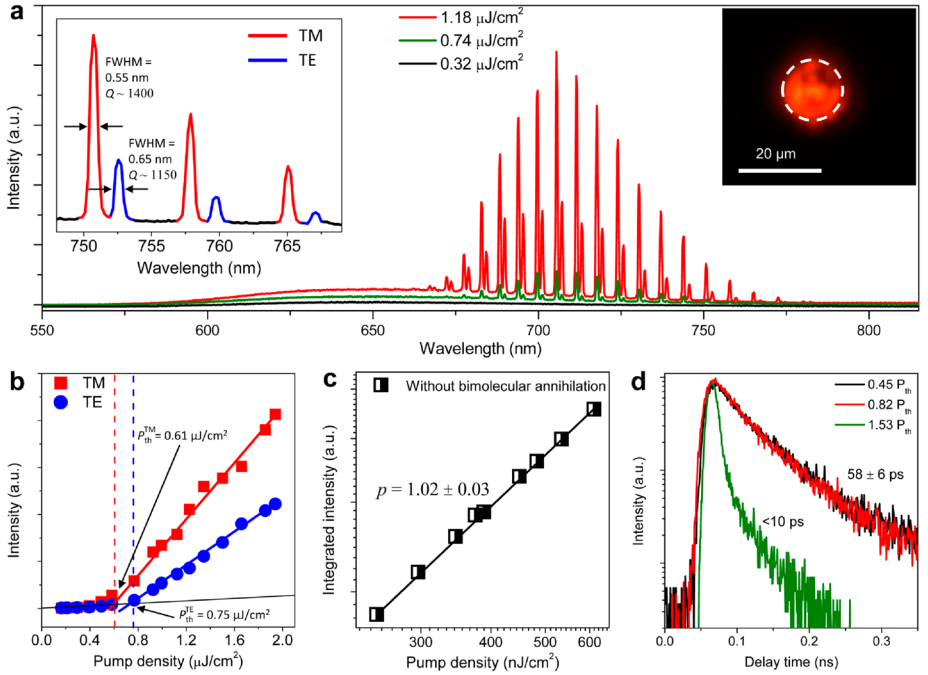

Figure 4. (a) The μ-PL spectra of one hemisphere with diameter D = 14.4 μm under different pump pulse energies, 0.32, 0.74, and 1.18 μJ/cm^2, at room temperature. Right inset: the magnified spectrum around 760 nm. Left inset: the PL microscopy optical image of this corresponding hemisphere above the lasing threshold. Scale bar is 20 μm. (b) Spectra intensity versus the pump power, which exhibits a TM mode threshold P_{th} of ~0.61 μJ/cm^2 and a TE mode threshold P_{th} of ~0.75 μJ/cm^2 respectively. (c) A plot of the integrated intensity versus the pump density below the lasing threshold, showing the linear emission regime (p = 1.02 ± 0.03) without exciton–exciton annihilation. (d) The decay files of PL at pump densities of 0.45, 0.82, and 1.53P_{th}.

DOI: 10.1021/jacs.5b03051
J. Am. Chem. Soc. 2015, 137, 9289–9295

Figure 4 provides the evidence of lasing from the individual DPHP hemisphere, optically pumped with a 400 nm femtosecond pulse laser by using our homemade micro-photoluminescence (μ-PL) setup (Figure S18). Figure 4a presents the μ-PL spectra of one single DPHP hemisphere with diameter D = 14.4 μm under different pump pulse densities. When the pump density exceeds a threshold from P = 0.32 (black line) to 0.74 (green line) μJ/cm^2, strong laser emission emerges as a set of sharp peaks on the top of the broad spontaneous spectrum line, the intensity of which rapidly increases with the further increasing of pump pulse energy. Impressively, the lasing emission peaks reach as far as ~780 nm in the NIR region. Additionally, impressive laser spots occur in the CCD-captured optical image of this single DPHP hemisphere above the lasing threshold, as shown in the right inset of Figure 4a. We found that a number of DPHP hemispheres exhibit bright laser spots (Figure S20) when a high pumping energy of ~5.1 μJ/cm^2 exceeds the lasing threshold of all hemispheres. At a closer look of the lasing spectra, the magnification of spectra around 760 nm (the left inset of Figure 4a) presents that the transverse magnetic (TM) modes and the transverse electric (TE) modes both exist within the DPHP spherical microcavity, which is precisely consistent with the characteristics of WGM cavity (Figure S21).[43,44] Furthermore, a plot of the intensities of emission spectra as a function of pump density, demonstrating a threshold at P_{th} = 610 nJ/cm^2, corresponding to the TM modes (red squares), is made in Figure 4b. And for TE modes (blue circles), the lasing threshold is ~750 nJ/cm^2, which is slightly larger than that of TE modes. In any event, the quality factor Q is an important parameter of a laser cavity, with the definition $Q = \lambda/\lambda_{fwhm}$, where λ is the peak wavelength and λ_{fwhm} is the fwhm of the lasing emission line. From the experiment, the Q factor is estimated to be as high as ~1.4 × 10^3 for TM mode, and ~1.2 × 10^3 for TE mode. In addition, the intensity of TE modes is lower than that of TM modes, which might be due to the higher Q factor of TM modes.[45]

In a realistic situation, the Q is determined by $1/Q = 1/Q_c + 1/Q_s + 1/Q_a$, where the first term $1/Q_c$ corresponds to the intrinsic photon leakage associated with the imperfect reflection resulting from the curvature of the circular cavity, $1/Q_s$ describes the loss due to light scattering from surface roughness, and $1/Q_a$ accounts for the absorption loss.[46] It is therefore understood that the Q factor of a WGM resonator is sensitively affected by its surface roughness and shape deformation. Our DPHP hemispheres with circular geometry provide the platform for the total internal reflection (TIR), which promise the low-leakage of photons (the first term $1/Q_c$). Meanwhile, the molecularly smooth surface (R_a ~ 1.5 nm) of DPHP hemisphere effectively prevents the light scattering associated with the second term $1/Q_s$. As for the third term $1/Q_a$, the existence of self-absorption is evident, as seen from the overlap between the absorption and PL spectra of DPHP single crystals (Figure 1a). Moreover, the self-absorption can account for the red-shifted lasing resonance peaks at longer wavelength (>700 nm), where there is sufficient optical gain without obvious self-absorption ($1/Q_a$) for lasing oscillator. Thus, the high-Q modes (~1.4 × 10^3) inherently arise from the perfectly circular shapes and the molecularly smooth surfaces of these self-assembled DPHP hemispheres.

A plot of the integrated intensities of emission spectra versus the pump intensities is exhibited in Figure 4c. The intensity dependence fits a power law x^p with p = 1.02 ± 0.03,[6] demonstrating a remain in the linear regime without bimolecular quenching (exciton−exciton annihilation). At the same time, Figure 4d shows the PL decay files at different pump intensities. As we can see, at intensities of 0.45P_{th} and 0.82P_{th}, the decay rates remain the same single exponential trend with τ of 58 ± 6 ps. It further confirms that there is no exciton−exciton annihilation with the increasing pump excitation. Further, the absence of bimolecular annihilation can be explained by the ultraefficient radiative transition in the J-aggregates of DPHP system. This radiative rate (k_r) of DPHP materials is as fast as ~1.98 × 10^9 s^{-1} that the optically pumped singlet excitons do not have enough time to diffuse through a few tenths to a few nanometers and collide with each other. Consequently, the exciton−exciton annihilation is absent in our DPHP solid-state hemispheres, which totally differentiates from the previously reported exciton−exciton annihilation under high excitation density in most of the organic materials systems, such as enthracene,[6] and p-distyrylbenzene.[29] Thus, in the case of DPHP hemispheres, the excitation energy can effectively contribute to the formation of the excitons in level 3 (Figure 2b), which completely transformed into the optical gain for lasing emission without exciton−exciton annihilation (the nonradiative channel). Therefore, the low lasing threshold of ~610 nJ/cm^2 is required for the population inversion to realize this organic NIR lasing. To further verify the laser action, we also investigated the PL lifetime of this hemisphere above the lasing threshold (green line, Figure 4d). Above the lasing threshold, for example, at 1.53P_{th} of TM modes, the PL decay time always collapses to <10 ps and is limited by the resolution of our apparatus. This short PL lifetime above the threshold suggests the process of lasing action occurs in this organic WGM cavity.[29] Besides, the absent exciton−exciton annihilation can prevent the device heating to some extent, which promises the optical stability of DPHP hemispheres under high carrier densities (Figure S19). As we know, this is also the first demonstration of nondoped organic solid-state NIR lasing without exciton−exciton annihilation.

The laser behaviors can be modulated through adjusting the size of the hemispheres (Figure 5). The μ-PL laser spectra of DPHP hemispheres with different sizes are presented in Figure 5a. For the lasing spectra of the WGM-type resonance, the mode spacing (between two adjacent TE or TM resonance mode peaks), $\Delta\lambda_m$, is given by

$$\Delta\lambda_m = \frac{\lambda^2}{L[n - \lambda(dn/d\lambda)]} \quad (3)$$

where L is the round-trip length within one hemisphere resonator (a function of diameter of hemisphere: $L = \pi D$), λ is the wavelength of the light, n is the phase refractive index of material, and $dn/d\lambda$ is the dispersion relation.[47] The mode spacing $\Delta\lambda_m$ between two adjacent peaks around 720 nm is 26.3 and 10.2 nm for these two corresponding hemispheres with diameters of 3.3, and 8.5 μm, respectively (Figure 5a). The increasing number of modes with the increasing size of hemispheres indicates that the optical modulation is certainly based on the confinement of photons within the hemispherical optical resonator. Figure 5b shows a plot of the mode spacing $\Delta\lambda_m$ versus $1/D$ of DPHP hemispheres, demonstrating clearly a linear relationship. Therefore, this linear relationship indicates the lasing mechanism is ascribed to WGM. And the bottom inset of Figure 5b demonstrates the simulated electromagnetic field distribution of one typical hemisphere (D = 3.3 μm),

DOI: 10.1021/jacs.5b03051
J. Am. Chem. Soc. 2015, 137, 9289−9295

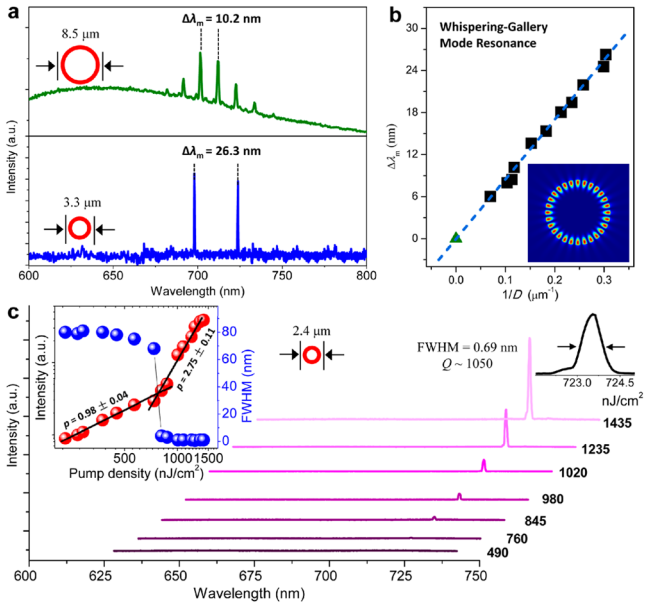

Figure 5. (a) The lasing spectra for two sample hemispheres with diameters of 8.5 and 3.3 μm. (b) The mode spacing $\Delta\lambda_m$ versus $1/D$, showing clearly a linear relationship. The bottom inset shows the simulated electric energy density time average (J/m^3, λ = 720 nm, n = 1.60) in the hemispherical resonator with D = 3.3 μm. Red corresponds to the highest field density and blue is the lowest field density. (c) Room-temperature PL spectra from one small DPHP hemisphere with D = 2.4 μm excited at different energies of 490, 760, 845, 980, 1020, 1235, and 1435 nJ/cm^2. Left inset: The integrated intensity (red spheres) and the fwhm (blue spheres) as a function of the optical pump density. The right inset shows the single high-Q mode (~1050), taken at 1435 nJ/cm^2.

which shows the excellent light-confinement in the spherical WGM resonator feedback. Note that WGM consists of both TE and TM modes. We found that for small-size hemispheres, such as that with D = 3.3 μm, only TM modes can be supported. In contrast, both TM and TE modes can be supported in large-size (>9.0 μm) DPHP hemispheres. Thus, the number of resonance lasing peaks and the specified polarized resonance modes (TM or TE modes) can be precisely modulated by the size of organic DPHP hemispheres.

As compared with these above-observed multimode lasing behavior, single-mode lasing has its immanent merits as good stability of laser oscillation due to the absence of mode competition, excellent monochrome properties of laser beam, and fine optical coherence.[48] In principle, the gain of lasing action is determined by the spatial spectra and the spectral overlap between the resonance and the gain material. Our "bottom up" method can allow the preparation of much smaller spherical microcavities than those previously reported WGM microcavities, resulting in fewer modes overlapping the DPHP emission than in larger hemispheres. Therefore, further decreasing the size of hemisphere, single-mode lasing was successfully achieved in the self-assembled DPHP hemisphere with D = 2.4 μm (Figure 5c). The lasing threshold P_{th} of ~780 nJ/cm^2 is identified as the intersection between the linear and the superlinear regions (red spheres, the left inset of Figure 5c). The linear regime (p = 0.98 ± 0.04) again strongly reveals the elimination of bimolecular quenching in the solid-state DPHP hemispheres. And the suplinear regime with p = 2.75 ± 0.11 indicates the process of lasing oscillator in this hemispherical WGM microcavity. Moreover, measurements of the line-width dependence on pump density show an abrupt decrease to a value limited by our instrument resolution soon after the changeover to superlinear behavior (blue spheres, in the left inset of Figure 5c). This single-frequency emission at ~723 nm has a high quality factor Q of ~1050 (the right inset of Figure 4c), which illustrates the efficient optical feedback with such small size (D = 2.4 μm). Thus, these organic hemispheres with small size (D < 2.8 μm) can provide the platform for the single-frequency near-IR coherent light sources.

CONCLUSION

Our work has demonstrated room-temperature NIR lasing with a low threshold based on self-assembled organic solid-state hemispheres. The amphiphilic nature of DPHP molecules contributes to the self-assembly of DPHP hemispheres, which inherently have perfect circular shapes and molecularly flat surfaces for the high-Q (~1.4 × 10^3) WGM optical microcavity. Due to the formation of the J-type molecular coupling components in the solid-state, the enhanced radiative decay rate k_r = (1.98 ± 0.29) × 10^9 s^{-1} of DPHP hemispheres promises the high optical gain and eliminates the exciton–exciton annihilation under high carrier densities, which has significantly allowed the realization of NIR lasing oscillator within the individual DPHP hemispheres. Furthermore, the ultralow NIR lasing threshold (~610 nJ/cm^2) of the DPHP hemispheres is attributed to the elimination of the exciton–exciton annihilation and the self-assembled high-Q WGM microcavity. Significantly, single-frequency near-IR lasing was successfully achieved in the DPHP hemispheres with small diameter (D < 2.8 μm). These easily fabricated organic solid-state hemispheres are the natural high-Q optical microcavities, which provide the platform for the low-threshold coherent light sources integrated on the microscale optics chip at the NIR wavelength. Together with the elimination of exciton–exciton annihilation under high carrier density, the high quantum efficiency, and the high-Q WGM hemispherical microcavity, our findings indicate that these self-assembled DPHP hemispheres may open up the directions for the worldwide race of achieving electrically pumped lasing in organic semiconductor materials.

ASSOCIATED CONTENT

Supporting Information

Experimental section, synthesis procedure, structure elucidation (^{1}H NMR, and ^{13}C NMR) of DPHP, cell structure of DPHP crystal, FT-IR measurement of DPHP solid form, optical measurements of the DPHP solution (in different solvents), the optical and fluorescence microscopy images of the as-prepared hemispheres, SEM image of the DPHP hemispheres, the numerically calculated absorption and PL spectra, the schematic illustration of the near-field scanning optical microscopy, the shot-dependent laser emission density of the DPHP hemisphere, and FDTD simulation of electromagnetic field distribution. The Supporting Information is available free of charge on the ACS Publications website at DOI: 10.1021/jacs.5b03051.

AUTHOR INFORMATION

Corresponding Author

*hongbing.fu@iccas.ac.cn

Notes

The authors declare no competing financial interest.

DOI: 10.1021/jacs.5b03051
J. Am. Chem. Soc. 2015, 137, 9289–9295

■ ACKNOWLEDGMENTS

This work was supported by the National Natural Science Foundation of China (nos. 91222203, 21273251, 91333111, 21190034, 21221002), project of State Key Laboratory on Integrated Optoelectronics of Jilin University (IOSKL2014KF16), project of Construction of Innovative Teams and Teacher Career Development for Universities and Colleges Under Beijing Municipality (IDHT20140512), the National Basic Research Program of China (973) 2011CB808402, 2013CB933500, and the Chinese Academy of Sciences.

■ REFERENCES

(1) Maiman, T. H. *Nature* **1960**, *187*, 493.
(2) Schafer, F. P.; Schmidt, W.; Volze, J. *Appl. Phys. Lett.* **1966**, *9*, 306.
(3) Tessler, N.; Denton, G. J.; Friend, R. H. *Nature* **1996**, *382*, 695.
(4) Kozlov, V. G.; Bulovic, V.; Burrows, P. E.; Forrest, S. R. *Nature* **1997**, *389*, 362.
(5) Samuel, I. D. W. *Nature* **2004**, *429*, 709.
(6) Kena Cohen, S.; Forrest, S. R. *Nat. Photonics* **2010**, *4*, 371.
(7) Samuel, I. D. W.; Turnbull, G. A. *Chem. Rev.* **2007**, *107*, 1272.
(8) Lidzey, D. G.; Bradley, D. D. C.; Skolnick, M. S.; Virgili, T.; Walker, S.; Whittaker, D. M. *Nature* **1998**, *395*, 53.
(9) Xu, Z.; Liao, Q.; Shi, Q.; Zhang, H.; Yao, J.; Fu, H. *Adv. Mater.* **2012**, *24*, OP216.
(10) Clark, J.; Lanzani, G. *Nat. Photonics* **2010**, *4*, 438.
(11) An, B.-K.; Gierschner, J.; Park, S. Y. *Acc. Chem. Res.* **2012**, *45*, 544.
(12) Lee, O. P.; Yiu, A. T.; Beaujuge, P. M.; Woo, C. H.; Holcombe, T. W.; Millstone, J. E.; Douglas, J. D.; Chen, M. S.; Fréchet, J. M. J. *Adv. Mater.* **2011**, *23*, 5359.
(13) Fang, H.-H.; Yang, J.; Feng, J.; Yamao, T.; Hotta, S.; Sun, H.-B. *Laser & Photon. Rev.* **2015**, *9*, 128.
(14) Qian, G.; Wang, Z. Y. *Chem. - Asian J.* **2010**, *5*, 1006.
(15) Caspar, J. V.; Kober, E. M.; Sullivan, B. P.; Meyer, T. J. *J. Am. Chem. Soc.* **1982**, *104*, 630.
(16) Shimizu, M.; Kaki, R.; Takeda, Y.; Hiyama, T.; Nagai, N.; Yamagishi, H.; Furutani, H. *Angew. Chem., Int. Ed.* **2012**, *51*, 4095.
(17) Özçelik, S.; Akins, D. L. *J. Phys. Chem. B* **1997**, *101*, 3021.
(18) Kozlov, V. G.; Burrows, P. E.; Parthasarathy, G.; Forrest, S. R. *Appl. Phys. Lett.* **1999**, *74*, 1057.
(19) Ma, Y.-Z.; Xiao, K.; Shaw, R. W. *J. Phys. Chem. C* **2012**, *116*, 21588.
(20) Howard, I. A.; Hodgkiss, J. M.; Zhang, X.; Kirov, K. R.; Bronstein, H. A.; Williams, C. K.; Friend, R. H.; Westenhoff, S.; Greenham, N. C. *J. Am. Chem. Soc.* **2010**, *132*, 328.
(21) Wheeler, D. A.; Zhang, J. Z. *Adv. Mater.* **2013**, *25*, 2878.
(22) Shaw, P. E.; Ruseckas, A.; Peet, J.; Bazan, G. C.; Samuel, I. D. W. *Adv. Funct. Mater.* **2010**, *20*, 155.
(23) Vahala, K. J. *Nature* **2003**, *424*, 839.
(24) Hood, C. J.; Kimble, H. J.; Ye, J. *Phys. Rev. A: At., Mol., Opt. Phys.* **2001**, *64*, 033804.
(25) Gérard, J. M.; Sermage, B.; Gayral, B.; Legrand, B.; Costard, E.; Thierry-Mieg, V. *Phys. Rev. Lett.* **1998**, *81*, 1110.
(26) Dharanipathy, U. P.; Minkov, M.; Tonin, M.; Savona, V.; Houdré, R. *Appl. Phys. Lett.* **2014**, *105*, 101101.
(27) Tamboli, A. C.; Haberer, E. D.; Sharma, R.; Lee, K. H.; Nakamura, S.; Hu, E. L. *Nat. Photonics* **2007**, *1*, 61.
(28) Chiasera, A.; Dumeige, Y.; Féron, P.; Ferrari, M.; Jestin, Y.; Nunzi Conti, G.; Pelli, S.; Soria, S.; Righini, G. C. *Laser Photonics Rev.* **2010**, *4*, 457.
(29) Wang, X.; Liao, Q.; Kong, Q.; Zhang, Y.; Xu, Z.; Lu, X.; Fu, H. *Angew. Chem., Int. Ed.* **2014**, *53*, 5863.
(30) Wang, X.; Li, H.; Wu, Y.; Xu, Z.; Fu, H. *J. Am. Chem. Soc.* **2014**, *136*, 16602.
(31) Vinogradov, S. N.; Linnel, R. H. *Hydrogen Bonding*van Nostrand Reinhold: New York, 1971.
(32) Luo, J.; Xie, Z.; Lam, J. W. Y.; Cheng, L.; Chen, H.; Qiu, C.; Kwok, H. S.; Zhan, X.; Liu, Y.; Zhu, D.; Tang, B. Z. *Chem. Commun.* **2001**, *18*, 1740.
(33) Chen, J.; Law, C. C. W.; Lam, J. W. Y.; Dong, Y.; Lo, S. M. F.; Williams, I. D.; Zhu, D.; Tang, B. Z. *Chem. Mater.* **2003**, *15*, 1535.
(34) Lkowicz, J. R. *Principles of fluorescence spectroscopy*; Springer, Berlin-Heidelberg, 2006.
(35) Sherwood, G. A.; Cheng, R.; Smith, T. M.; Werner, J. H.; Shreve, A. P.; Peteanu, L. A.; Wildeman, J. *J. Phys. Chem. C* **2009**, *113*, 18851.
(36) Würthner, F.; Kaiser, T. E.; Saha-Möller, C. R. *Angew. Chem., Int. Ed.* **2011**, *50*, 3376.
(37) Spano, F. C. *Acc. Chem. Res.* **2010**, *43*, 429.
(38) Krueger, B. P.; Scholes, G. D.; Fleming, G. R. *J. Phys. Chem. B* **1998**, *102*, 5378.
(39) Chen, R.; Van Duong, T.; Sun, H. D. *Sci. Rep.* **2012**, *2*, 2.
(40) Kiraz, A.; Sennaroglu, A.; Doğanay, S.; Dündar, M. A.; Kurt, A.; Kalaycıoğlu, H.; Demirel, A. L. *Opt. Commun.* **2007**, *276*, 145.
(41) Qian, S. X.; Snow, J. B.; Tzeng, H. M.; Chang, R. K. *Science* **1986**, *231*, 486.
(42) Xu, Z.; Liao, Q.; Shi, X.; Li, H.; Zhang, H.; Fu, H. *J. Mater. Chem. B* **2013**, *1*, 6035.
(43) Haase, J.; Shinohara, S.; Mundra, P.; Risse, G.; Lyssenko, V. G.; Fröb, H.; Hentschel, M.; Eychmüller, A.; Leo, K. *Appl. Phys. Lett.* **2010**, *97*, 211101.
(44) Yim, T.-J.; Zentgraf, T.; Min, B.; Zhang, X. *J. Am. Chem. Soc.* **2010**, *132*, 2154.
(45) Hosoda, M.; Shigaki, T. *Appl. Phys. Lett.* **2007**, *90*, 181107.
(46) Fang, H.-H.; Ding, R.; Lu, S.-Y.; Yang, Y.-D.; Chen, Q.-D.; Feng, J.; Huang, Y.-Z.; Sun, H.-B. *Laser & Photon. Rev.* **2013**, *7*, 281.
(47) Wang, X.; Liao, Q.; Lu, X.; Li, H.; Xu, Z.; Fu, H. *Sci. Rep.* **2014**, *4*, 7011.
(48) Gao, H.; Fu, A.; Andrews, S. C.; Yang, P. *Proc. Natl. Acad. Sci. U. S. A.* **2013**, *110*, 865.

DOI: 10.1021/jacs.5b03051
J. Am. Chem. Soc. 2015, 137, 9289−9295